

Three-dimensional shapes and spatial distributions of Pt and PtCr catalyst nanoparticles on carbon black

L. CERVERA GONTARD*[†], R.E. DUNIN-BORKOWSKI[†]*
& D. OZKAYA[‡]

*Department of Materials Science and Metallurgy, University of Cambridge, Pembroke Street, Cambridge CB2 3QZ, U.K.

[†]Center for Electron Nanoscopy, Technical University of Denmark, DK-2800 Kongens Lyngby, Denmark

[‡]Johnson Matthey Technology Centre, Blount's Court, Sonning Common, Reading RG4 9NH, U.K.

Key words. Heterogeneous catalysts, nanoparticle shapes, nanoparticles, platinum, platinum alloy, tomography.

Summary

High-angle annular dark-field scanning transmission electron microscopy tomography is applied to the study of Pt and PtCr nanoparticles supported on carbon black, which are used as heterogeneous catalysts in the electrodes of proton exchange membrane fuel cells. By using electron tomography, the three-dimensional architecture of the heterogeneous catalyst system can be determined, providing high-spatial-resolution information about the shapes, faceting and crystallographies of 5–20 nm single and multiply twinned catalyst particles, as well as their positions with respect to the carbon support. Approaches that can be used to provide improved information about the distribution and orientation of the particles on their support are proposed and discussed. Our results show that electron tomography provides important information that is complementary to high-resolution lattice imaging. Both techniques are required to understand fully the nature and role of the surfaces of faceted catalyst particles.

Introduction

Catalysts mediate chemical reactions, enabling the highly selective formation of desired products at increased rates (Bowker, 1998; Bell, 2003; Kolasinski, 2004). The majority of industrial catalysts are heterogeneous, taking the form of high-surface-area solids onto which an active component is dispersed in the form of very small particles. For example, proton exchange membrane fuel cells typically require high loadings of platinum and must be able to provide good electrical conductivity, reactant gas access, water handling and corrosion resistance. As the support helps to disperse the

particles evenly and to prevent them from coalescing, it is important to optimize the three-dimensional distribution of the particles in the matrix. In addition, the accessibility of the supported nanoparticles to reactant molecules is determined by their location with respect to the support, and in particular whether they are on the surface of the support or embedded within it. Electrocatalysts with high dispersions are typically supported on mesoporous high-surface-area ($>75 \text{ m}^2 \text{ g}^{-1}$) carbon blacks. Carbon blacks are low-grade forms of graphite that are usually composed of spherical crystallites and lack three-dimensional order. The crystallites in most commercial carbon blacks average approximately four graphene layer planes in thickness (Heidenreich *et al.*, 1968; Burden *et al.*, 1998).

The shapes of the metal nanoparticles are known to play a highly important role in determining the performance of supported metal catalysts. In structure-sensitive catalytic reactions, only certain parts of the surfaces of metal nanoparticles contain dominant active sites for the desired products; the other faces are then either inactive or active for producing undesired side products. The structures and shapes of metallic nanoparticles have been studied intensively both theoretically and experimentally (Marks, 1994). The equilibrium shape of a nanoparticle can be obtained by minimizing its surface energy. Metallic particles often have morphologies that are approximately consistent with a Wulff construction. For a single crystal with a face-centred cubic (fcc) structure, such as platinum, the equilibrium crystal shape at 0 K is a truncated octahedron that contains only (111) and (100) facets, whereas at temperatures above 0 K other low-index facets, such as (110) are frequently present. The relative extension of the planes then depends on the anisotropy ratio of the surface energies between different planes. This ratio can change, typically taking a value close to unity near the melting point of a crystal (Yacamán & Domínguez, 1980;

Correspondence to: Lionel Cervera Gontard. Tel: +45 4525 6469; fax: +45 4588 0307; e-mail: lionel.gontard@cen.dtu.dk

Graoui *et al.*, 1998), resulting in rounder particle shapes at higher temperatures.

There is known to be a strong relationship between the sizes and the shapes of platinum particles, which results in the fraction of 100-type surfaces decreasing with increasing particle size (Wang *et al.*, 1985; Topsøe, 2003). Such changes can, in turn, affect catalytic activity. In practice, the shapes of particles may show strong deviations from Wulff shapes as a result of kinetic growth effects (Marks, 1985). For example, alternative equilibrium shapes are frequent for gold clusters, including the formation of multiply twinned particles and amorphous structures (Ascencio *et al.*, 1998). In addition, the presence of adsorbates can affect surface energies.

Transmission electron microscopy (TEM) tomography has become an established technique in the study of materials. However, bright- and dark-field TEM images, which may be suitable for biological electron tomography, rarely provide useful signals for electron tomography of strongly diffracting crystalline specimens of inorganic materials. Alternatively, tomography can be performed in a TEM using energy-filtered images and weak-beam dark-field imaging. Examples of the application of these techniques include studies of nanocomposites of FeAl + Y₂O₃, carbon nanotubes, Si particles embedded in SiO_x, scanning tunnelling microscopy probes, polyhedral particles of CeO₂, polymers and dislocations (Möbus & Inkson, 2001; Gass *et al.*, 2006; Barnard *et al.*, 2006; Jinnai *et al.*, 2006; Yurtsever *et al.*, 2006; Xu *et al.*, 2007a).

By contrast to the use of TEM, if an image is obtained at medium resolution using high-angle annular dark-field scanning transmission electron microscopy (HAADF STEM), then the effects of diffraction contrast are much weaker, and the recorded signal can vary monotonically with both composition and specimen thickness, providing a better approximation to the projection requirement for tomography (Midgley *et al.*, 2006, 2007; Weyland *et al.*, 2006). This technique is especially suitable for high-atomic number catalyst nanoparticles supported on low-atomic number supports, as has been reported previously (Weyland *et al.*, 2001, Gontard *et al.*, 2005; Uchida *et al.*, 2006, Wikander *et al.*, 2007).

Here, we use HAADF STEM tomography to study Pt and PtCr particles supported on carbon black, which are used as heterogeneous catalysts in proton exchange membrane fuel cells. The shapes of particles with sizes of between 5 and 20 nm are determined, and approaches that can be used to measure the distributions of the particles on their support are assessed.

HAADF STEM tomography: reconstruction artefacts, beam damage and spatial resolution

Electron tomography has been used in the biological sciences for more than 30 years to obtain three-dimensional information from two-dimensional projections of a structure. The two-dimensional projections that are used for

reconstruction must meet the 'projection requirement', that the signal collected should be an integral through the structure of some physical property. The technique involves: (1) the acquisition of a tilt-series of projections of the specimen; (2) reconstruction of the three-dimensional volume using a chosen algorithm and (3) processing and visualization of the three-dimensional data. Although different specimen tilting geometries are possible, the most simple of these for electron microscopy is single-axis tilting. The specimen must be tilted about the eucentric axis of the specimen holder rod over a tilt range that is as close to $\pm 90^\circ$ as possible. The greater the number of images and the tilt range, the better the fidelity of the final reconstruction of the three-dimensional volume. In practice, the maximum tilting range in the experiments described below is limited to $\pm 80^\circ$ by the microscope goniometer. The maximum tilt range can also be limited by overlap of the specimen or the grid bars onto the area of interest when the holder is tilted to high angles.

Tomographic reconstructions can exhibit artefacts resulting from a combination of: (1) poorly spatially registered projections; (2) limited tilt angles, leading to a distortion in the direction of the 'missing wedge' (see below) and anisotropic resolution; (3) obscuring of specimen details by contamination and (4) the choice of reconstruction algorithm, which may enhance certain specimen features over others. In Friedrich *et al.* (2005), intensity distributions in tomograms determined from bright-field TEM, ADF STEM and HAADF STEM images of magnetite nanocrystals were compared to determine the influence of tilt angle, tilt increment, diffraction contrast, noise and reconstruction algorithm [weighted backprojection and simultaneous iterative reconstruction techniques (SIRT)] on the quality of the reconstruction. Noise was found to play the most important role in degradation of the reconstruction if the tilt range was sufficient. Although a carbon support film can introduce noise, its contribution to the signal can sometimes be subtracted before reconstruction. However, if the carbon support is thick, then it can introduce artefacts in a reconstruction such as the top-bottom effect as described by Yang *et al.*, 2005. Another consequence of prolonged exposure to the electron beam may be contamination from hydrocarbons. The presence of adsorbed hydrocarbon molecules on the specimen surface can result in the formation of a carbon-rich polymerized film. The growth rate of this film is proportional to the current density and the irradiation time. Figure 1 shows STEM HAADF images of the same area of a sample of platinum particles on carbon both before and after the acquisition of a tomographic tilt series. The severe contamination shown in Fig. 1 greatly affects the noise level in the HAADF signal, reducing the resolution and the fidelity of the final tomographic reconstruction.

The spatial resolution d of a tomographic reconstruction is related to the number of images acquired in the tilt series and to the diameter of the volume to be reconstructed. For a single tilt axis, the resolution of the reconstruction is different in each

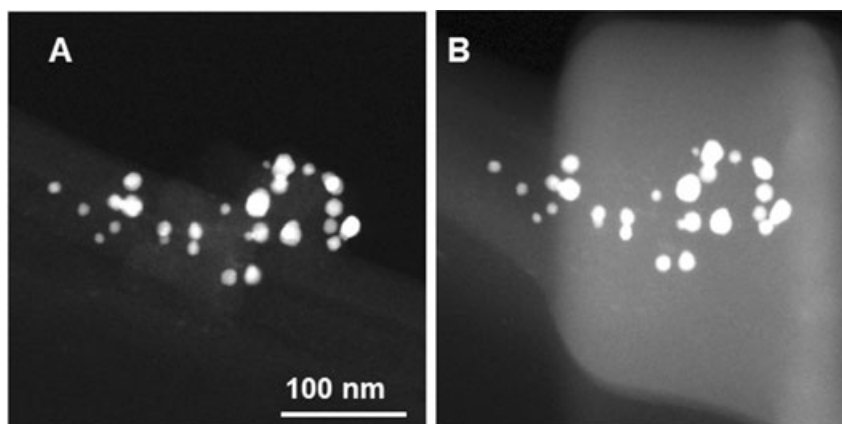


Fig. 1. (A) HAADF STEM image of Pt nanoparticles on carbon. (B) The same area after tomographic acquisition of 120 images, showing a thick layer of contamination.

spatial direction. The resolution parallel to the tilt axis, d_x , is equal to the resolution of the original projections, assuming perfect tilt series alignment. The resolution in the direction perpendicular to the tilt axis, d_y , is controlled by the number of projections acquired, N , and the diameter of the volume to be reconstructed, D . Crowther *et al.* (1970) stated that

$$d_y = \frac{\pi D}{N} \quad (1)$$

This expression assumes that N projections cover a tilt range of $\pm 90^\circ$. The resolution in the third direction, d_z (the depth direction) is degraded further by an elongation factor which is related to the maximum tilt angle, α and varies between 1.9 and 1 for maximum tilt angles of $\pm 50^\circ$ and $\pm 90^\circ$, respectively.

HAADF STEM tomography requires the use of long exposure times, and the high current density in the STEM probe should theoretically result in great damage to specimens. Electron beam damage is a common problem for many specimens and can take the form of displacement of atoms from their sites, strain resulting in local crystal tilt, and a gradual reduction in image contrast. Elastic 'knock-on' damage dominates in conducting samples, but the threshold voltage for atomic displacement collisions in metals of high atomic number (such as Pt) is greater than the 200 kV accelerating voltage used in the present experiments. Knock-on damage is more important in the case of carbon, but the carbon support used in this research is intrinsically amorphous, and the effects of damage are not obvious experimentally. In specimens that can be damaged by local heating, STEM can minimize the damage caused, as the electron dose is much lower than for conventional TEM imaging, and rastering of the probe allows dissipation of heat (phonons) into surrounding non-illuminated areas. Pt particles on carbon supports are in many ways ideal for STEM HAADF tomography because of the large difference in atomic number between carbon and platinum, and also because they are relatively resistant to beam damage. By contrast, other samples, such as mesoporous catalysts, can be beam sensitive, and successful acquisitions are then

only possible when exposure to the beam is minimized, at the expense of increased noise.

Experimental details

Carbon-supported (Vulcan XC-72R) platinum (19.1 wt%) was prepared using established techniques that are described elsewhere (Ralph & Hogarth, 2002; Ozkaya *et al.*, 2003). The samples were further reduced in a N_2 -rich atmosphere at 900°C . In part to reduce the overall cost of the catalyst, alloys of Pt with metals are also used frequently. Significantly, some of these alloys have been found to enhance catalytic activity when compared with that of pure Pt for oxygen reduction at the cathodes of fuel cells. It is thought that the addition of base metals may prevent restructuring of atoms on the surface of the particles during oxygen reduction. Here, in addition to particles of pure Pt, two alloys comprising 40 wt% of PtCr particles on carbon black with a Pt:Cr atomic ratio of 50:50, were examined using HAADF STEM tomography.

The specimens studied here were prepared as dry powders and examined on holey carbon copper TEM grids. Experimental data were acquired on a Tecnai F20 Super Twin field-emission gun TEM operated in scanning mode at 200 kV using camera lengths of between 100 and 490 mm (corresponding to inner HAADF detector semi-angles of between 50 and 10 mrad). The following parameters were used: extraction voltage 3.8 kV; gun lens 6; spot size 7; 70 μm condenser aperture. These settings correspond to a probe diameter for STEM imaging of approximately 0.20–0.25 nm and a current density of $0.6 \text{ pA}/\text{\AA}^2$. The dwell time was 10 $\mu\text{s}/\text{pixel}$ (40 s/1024 \times 1024 pixel image), corresponding to an electron dose of $70 \text{ e}^-/\text{\AA}^2$ at each tilt angle. The images were acquired using a Fischione Instruments (Export, PA, USA) 2020 single-tilt tomography holder with a maximum tilt range of $\pm 80^\circ$ limited by the microscope goniometer. Alignment of the images and tomographic reconstruction using SIRT (15–20 iterations proved to be sufficient to achieve convergence) were performed using the software *Inspect3D*.

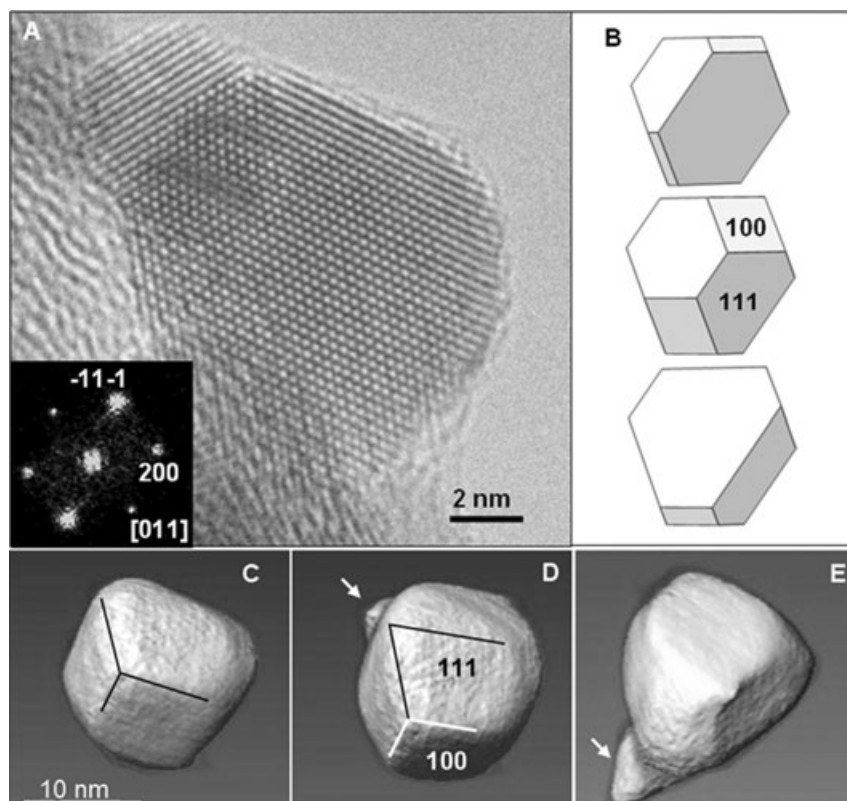


Fig. 2. (A) Conventional HRTEM image of overlapping Pt nanoparticles on carbon. A diffractogram showing the orientation of the larger particle is shown in the inset. (B) Schematic diagrams illustrating the fact that three particles can have the same outlines but different three-dimensional morphologies (C–E). Three views of an isosurface reconstruction of a 15 nm Pt particle obtained using HAADF STEM tomography, with an inner detector semi-angle of 50 mrad, a tilt range of $\pm 75^\circ$ and a tilt increment of 1° . The white arrows in (D) and (E) indicate artefacts from the reconstruction.

Visualization of the final three-dimensional datasets was performed using *Amira V2.3* software. Isosurface rendering was used to display Pt particles, whereas the carbon support was processed separately by performing manual segmentation. Although the latter procedure is subjective, it generally provides better results than using an isosurface. In addition, in contrast to using a voxel projection, it allows quantification of parameters such as the area and volume of the resulting three-dimensional structure.

The use of a Fischione Instruments plasma cleaner (model 1020) before acquisition, typically for 10–30 s, was used to minimize the build-up of contamination. Care was taken to ensure that variations in intensity could not be attributed to an appreciable increase in the presence of hydrocarbons. Apart from occasional problems with contamination, changes to the areas of interest were not observed during acquisition of tomographic tilt series.

Results and discussion

Shapes of platinum particles

HAADF STEM tomography has been applied previously to the determination of the shapes of individual nanoparticles,

including magnetite crystals (Buseck *et al.*, 2001), CeO₂ particles (Xu *et al.*, 2007b) and quantum dots (Arslan *et al.*, 2005). Here, in order to use HAADF STEM tomography to measure the shapes of Pt catalyst nanoparticles with sufficient spatial resolution, magnifications of between 910 kx and 1.8 Mx were used. In order to minimize diffraction contrast, the camera length was set to 100–150 mm, corresponding to inner detector semi-angles of 50–45 mrad. Figure 2(A) shows a conventional high-resolution TEM (HRTEM) image of overlapping Pt particles with sizes of below 10 nm, acquired at 400 kV using a JEOL 4000EX TEM. Such images contain important information about crystalline structure, but they contain limited information about the particle volume and shape (Marks & Smith, 1983; Marks, 1984). Although some depth information can be inferred from HRTEM images of Pt nanoparticles (Gontard *et al.*, 2007), such experiments are not conclusive and the particles have to be imaged at zone-axis orientations. Figure 2(B) illustrates the fact that Pt particles with highly different morphologies can have identical outlines (and similar HRTEM image contrast). In striking contrast to Fig. 2(A), Fig 2(C–E) shows the results of applying HAADF STEM tomography to recover the three-dimensional morphology of a 15 nm Pt particle (not the same particle as in Fig. 2A) from a tilt-series of images acquired using a

magnification of 1.3 Mx, over a tilt range of $\pm 75^\circ$ and a tilt increment of 1° . Three views of an isosurface visualization of the particle are shown in Fig. 2(C–E). The angles between certain facets could be measured from the reconstructed volume and were found to be consistent with values such as the 129.5° angle expected between 111 and 100 planes in platinum, whereas the overall particle shape was found to be an irregular truncated octahedron. It should be noted that the approach used to obtain and visualize the reconstruction shown in Fig. 2(C–E) provides images that contain almost no information about the particle support, whose intensity is very low in the original HAADF images. Possible approaches for imaging both the particles and their support in tomographic reconstructions are described below.

Figure 3 shows similar results obtained from a STEM HAADF tomographic series acquired over a tilt range of -70° to $+66^\circ$ with a tilt increment of 1° , at a magnification of 1.8 Mx using a camera length of 200 mm. We found that when higher magnification values were used instabilities of the sample and the electron beam, as well as contamination, were unavoidable. The spatial resolution in Fig. 3 can be estimated by substituting the values $D = 10$ nm (diameter of the reconstruction volume), and $N = 136$ (the number of images acquired within the range of angles: $+70^\circ$ to -66°) into Eq. 1, resulting in a value of 0.23 nm. The experimental spatial resolution will be lower because Eq. 1 is strictly valid for a tilt range of $\pm 90^\circ$. Although the carbon support in Fig. 3 is again not visible in the isosurface visualizations, Fig. 3(C) demonstrates for three 5–7 nm particles that HAADF STEM tomography can be used successfully to image the morphologies of sub-10 nm Pt particles, with an apparent resolution that is better than 1 nm.

However, it is also important to note that the use of a single isosurface contour for visualization masks the presence of rounding and artefacts associated with the tomographic point spread function that result from a limited tilt range and finite tilt increment. These effects, which may be pronounced in the direction of the incident electron beam when the specimen is not tilted, are apparent in line profiles generated from the reconstructed volume of a particle (Fig. 3D and E) and also account in part for the difficulty of visualizing the lower intensity carbon support at the same time as the heavier particles.

In the examples shown above, the edges between the facets on the Pt particles appear to be rounded in the reconstructions. Although some of this rounding is associated with the tomographic point spread function and with the presence of the surrounding carbon, the Pt samples examined in this study were annealed at 900°C . Reduction in different gases at high temperatures is normally used to make industrial heterogeneous catalyst particles, and to a degree the rounded edges seen experimentally may be a true feature and not an artefact. High-temperature annealing of palladium particles in oxygen is known to induce flattening and an extension of (100)

faces (Graoui *et al.*, 1998). Interestingly, these morphological variations are reversible after reduction in hydrogen. Platinum particles that are supported on silica or alumina form predominantly (100) crystal planes if they are grown in pure hydrogen. By contrast, when they are grown in air or nitrogen, they are more rounded or cuboctahedral (Wang *et al.*, 1985). Molecular dynamics simulations performed as a function of temperature have been used to demonstrate that the edges of gold particles tend to become rounder when the temperature is raised, with the appearance of higher index facets that include 110 facets, whereas 111 facets remain very stable even at high temperature (Wang *et al.*, 2004). Additionally, careful experiments combining HRTEM imaging and exit-wave restoration have been used to confirm that the edges of small particles may be stepped, and that surface atoms on nominally flat surfaces can in fact form islands and terraces (Gontard *et al.*, 2007). Neither truly flat faces nor atomically sharp edges are likely to be present on the Pt nanoparticles examined here. The rounding seen in the results from HAADF STEM tomography is likely to arise from a combination of the presence of low-index facets (such as 110 facets) with low surface area, true steps and terraces, and artefacts of the reconstruction and visualization process.

Figure 4 illustrates the fact that, with care, *the same* Pt particle can be located and observed using two techniques on two different microscopes. Figure 4(A) shows a high-resolution lattice image of an 8 nm Pt particle acquired using a JEM-2200 FS (Tokyo, Japan) TEM close to a $[110]$ zone-axis orientation. Figure 4(B) shows an isosurface visualization of the three-dimensional shape of *the same particle* obtained using HAADF STEM tomography on a Tecnai F20 TEM. The two techniques provide complementary crystallographic and morphological information about the particle, whose approximate orientation and shape are shown in Fig. 4(C). The size of the particle in the tomographic reconstruction is confirmed by counting the 111 lattice fringes of the HRTEM image, which have a known spacing of 0.2268 nm. By combining the three-dimensional particle shape obtained using tomography, and the information from the original tilt series of HAADF images, it is possible to obtain both the orientation and the shape of the particle. The particle shape was estimated by comparing different projections and measuring the corresponding edges of the different facets of the particle. The four HAADF images shown in Fig. 4(D), which were obtained at different tilt angles, illustrate the fact that the morphology of the particle corresponds approximately to the Wulff shape of a cuboctahedron. The first and fourth projections in Fig. 4(D) show hexagonal profiles with sharp edges close to a $[110]$ zone-axis orientation, bounded by 111- and 100-type facets. Because of limited spatial resolution, the rounded edges visible in Fig. 4(B) cannot be unambiguously attributed to real features such as steps or low-index 110 facets.

Small particles with fcc structures, particularly gold and silver, can sometimes have shapes that are not truncated

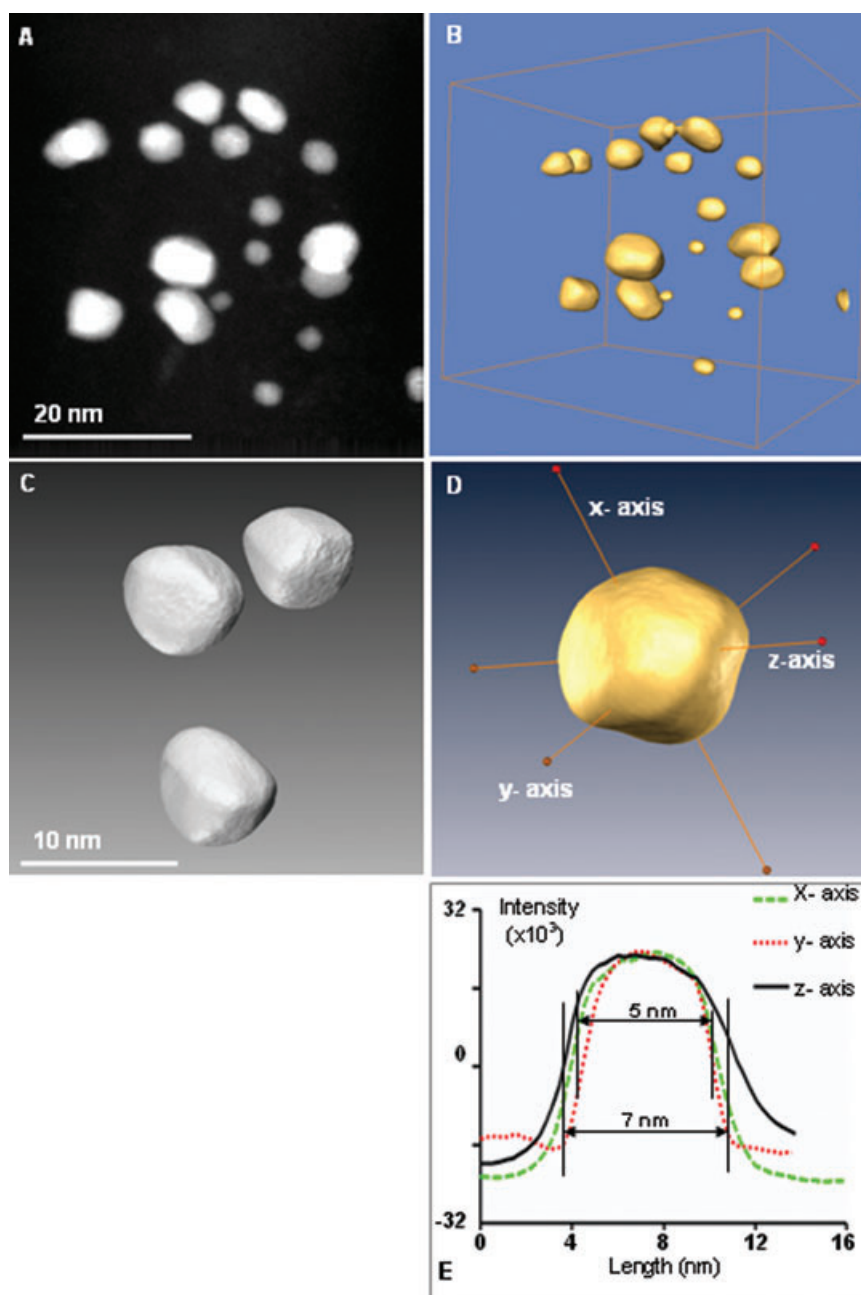


Fig. 3. (A) HAADF image of Pt particles on carbon. The signal from the carbon support is much lower than that from the particles. (B) Isosurface visualization of a tomographic reconstruction of the Pt particles shown in (A). (C) and (D) show selected particles from (B), on which faceting is apparent. (E) Line profiles taken along three orthogonal directions through the tomographic reconstruction of the particle shown in (D). The z-axis corresponds to the direction of the incident electron beam at a specimen tilt angle of 0° . The threshold used for visualization corresponds approximately to a decrease of 50% of the signal intensity.

single crystals, as a result of the fact that they can be multiply twinned. Twins are formed when coherence is achieved in the plane of the interface but the crystallographic axes in the material on opposite sides of the interface are related by a symmetry operation. Such particles can sometimes be composed of five units, yielding a decahedral shape, or twenty

units, yielding an icosahedral shape. They are typically built up of inhomogeneously strained single crystal units (Howie & Marks, 1984), with equilibrium shapes that can be obtained through the application of a modified form of the Wulff construction (Marks, 1983; Van de Waal, 1996). It also common to find fcc particles that are twinned symmetrically

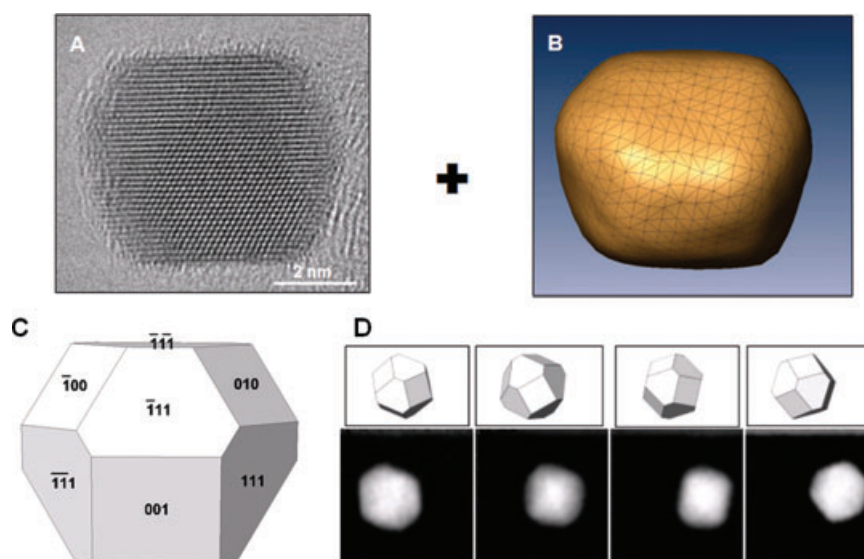


Fig. 4. (A) Conventional HRTEM image of an 8 nm Pt particle acquired on a JEM-2200FS TEM at 200 kV close to optimum defocus with C_s adjusted to $-20 \mu\text{m}$. (B) Isosurface visualization of the three-dimensional shape of the *same* particle obtained on a Tecnai F20 TEM using HAADF STEM tomography. (C) Schematic diagram showing the approximate crystallographic details of the same Pt particle, obtained by combining the information in (A) and (B). (D) Selection of four HAADF images of the particle shown in (A) and (B), acquired at different tilt angles (part of a series of 61 images), and the corresponding Wulff shapes (top).

into two units, by 111 planes. Figure 5 shows HAADF STEM results obtained from a Pt particle that contains a lamellar triple twin. Such twins were observed primarily in larger particles. Higher-order twin boundaries such as that shown in Fig. 5 can be modelled simply by changing the directions and magnitudes of twin facets, and the model is then independent of the exact form of the Wulff construction (Marks, 1983). Diffraction contrast from the twin is almost absent in the HAADF image shown in Fig. 5(B). However, the ADF image shown in Fig. 5(A) contains diffraction contrast associated with the presence of twinning and strain. The overall shape of the particle corresponds approximately to a cuboctahedron, in which the twin planes are parallel to opposite 111 facets of the particle. The corresponding HAADF STEM tomographic reconstructions of the particle are shown in Fig. 5(C–F).

Particle distribution on carbon support

The morphologies of many heterogeneous catalyst supports are complex, with rough surfaces and tortuous, interconnected pores that increase their exposed surface area (Sattler & Ross, 1986). When adsorption methods (in combination with the metal content of the supported catalyst) are used for measuring particle size distributions, if an appreciable fraction of the metal surface is inaccessible, then the particle size derived will be larger than the true particle size. X-ray diffraction techniques used for particle size measurement yield information averaged over millions of particles, and thus in principle provide better statistics than

TEM, but correlation with TEM is still frequently needed. The application of HAADF STEM tomography to heterogeneous catalysts can in principle overcome these limitations. The technique has previously been used to determine the spatial distributions of Pd-Ru bimetallic nanocatalysts within the pores of an SiO_2 matrix (Weyland *et al.*, 2001; Weyland, 2002), the active phase distribution of nafion ionomer-coated Pt/C used in the electrodes of polymer electrolyte fuel cells (Uchida *et al.*, 2006), and the incorporation of Pt particles in ordered mesoporous carbon (Wikander *et al.*, 2007).

When applying HAADF STEM tomography to Pt nanoparticles supported on carbon, the parameters that are of primary interest are the shapes and sizes of the particles and their distribution and interaction with the support. Unfortunately, it is difficult to obtain all of this information in a single experiment because the particles have high atomic number and are crystalline, whereas the support has low atomic number and is amorphous. On the assumption that the HAADF signal is approximately proportional to Z^2 , Pt ($Z = 78$) scatters 169 times more strongly than carbon ($Z = 6$). Figure 6 shows a comparison of three images of the same distribution of Pt nanoparticles on a carbon support acquired using (1) HAADF (with an inner detector cut-off semi-angle of 50 mrad), (2) ADF and (3) bright-field detectors in scanning mode. Neither the ADF nor the bright-field image is suitable for accurate and precise tomographic reconstruction of the individual particles, as diffraction contrast would result in larger artefacts than for HAADF tomography extending into the matrix if reconstruction of the particles were attempted.

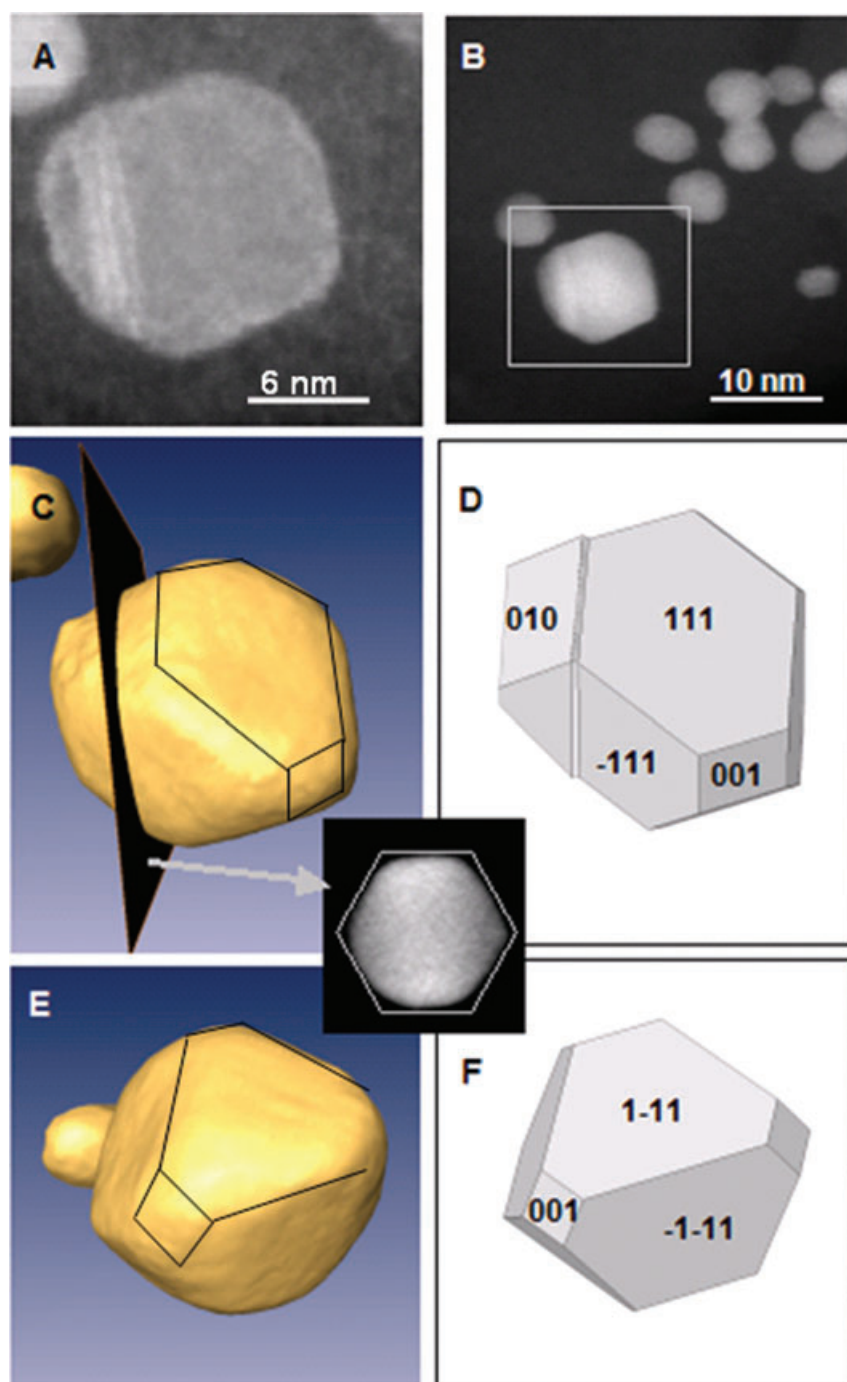


Fig. 5. (A) ADF STEM image of the Pt particle shown in (B), acquired at higher magnification and using a camera length of 490 mm (corresponding to an inner collection semi-angle of 20 mrad). Bright contrast in the particle arises from lamellar twinning. (B) HAADF STEM image of Pt particles taken from a tilt series acquired at 200 kV using a tilt range of $\pm 70^\circ$ and a tilt increment of 2° using a magnification of 1.3 Mx and a camera length of 200 mm (50 mrad). (C) and (E) Two different views of an isosurface visualization of the three-dimensional shape of the particle shown in (A) determined using HAADF STEM tomography. (D) and (F) Corresponding views of the inferred modified Wulff construction. The inset between images (C)–(F) shows that a section taken through the reconstruction at the position of the twin is approximately hexagonal in shape.

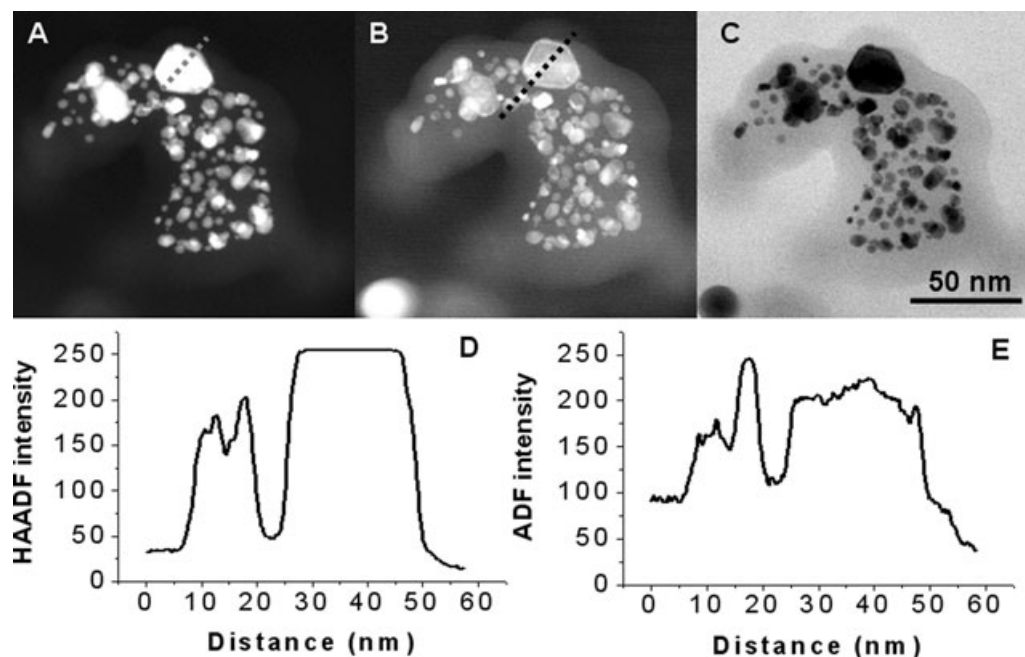


Fig. 6. (A) HAADF (inner detector semi-angle, 50 mrad), (B) ADF (inner detector semi-angle 10 mrad) and (C) bright-field images of a distribution of Pt particles, acquired at 200 kV. (D) and (E) are profiles of the signals acquired along the lines drawn on images (A) and (B), respectively.

Conversely, the HAADF signal collected may be optimal for recovering the shapes of the particles, but not the details of the weakly scattering support. Although changing the inner cut-off angle by increasing the camera length can be used to enhance the signal from the support, diffraction contrast can then be a problem for recovering the shapes of the particles. The detector can also be adjusted to enhance the HAADF signal from the carbon matrix, as shown in Fig. 6(A), but the Pt particles may then be saturated and artefacts may again result during the reconstruction of the carbon matrix. A number of solutions to these issues are possible. For example, HAADF tomography can be used to reconstruct the three-dimensional particle shapes and positions, and their relationship to the support can then be inferred qualitatively by observing either ADF or bright-field tilt series of images visually. Alternatively, digital image processing techniques can be used to remove the Pt particles from each image in an HAADF tilt series, to interpolate the matrix across the positions of these particles, and then to reconstruct the shape of the matrix alone, for visualization together with the particle shapes and positions determined using conventional HAADF STEM tomography. In the present study it was found experimentally that a compromise between these requirements could be achieved by using a relatively low inner detector semi-angle, approaching 10 mrad, to recover both the positions of the particles (but not their detailed shapes) and the shape of the support in the same experiment even if the signal from the particles was saturated. In Figs 7 and 8, for which inner cut-off angles of 40 and 10 mrad respectively were used, both

the positions and the approximate shapes of most of the PtCr particles are reconstructed and visualized together by combining surface segmentation and isosurface visualization with different threshold levels. Figures 7 and 8 correspond to two different samples that had been treated at different temperatures and in different atmospheres. The fraction and distribution of particles on the surface of the matrix was found to be very similar in each case and the reconstructions reveal that most of the PtCr particles are on the outer surfaces of the supports. Information of this type is important for quantifying the fraction of the particles that may be active for catalysis, i.e. those that are in direct contact with the reactant gases.

Our experiments show that, when samples of PtCr on carbon black supports are examined using HAADF STEM tomography, the positions and approximate shapes of the particles and the shape of the support can be recovered in three dimensions simultaneously. Such measurements are more challenging for Pt than for PtCr particles on the same supports, and the final reconstructions contained greater numbers of artefacts. Our results suggest that the ratio of atomic densities between the active phase and the support plays a key role in determining the fidelity, precision and accuracy of tomographic reconstructions of particle shapes and positions with respect to a low atomic number matrix, especially for particles that are below 10 nm in size. Combinations of different tomographic measurements and substantial image analysis and image processing may be required to improve such measurements significantly in future studies.

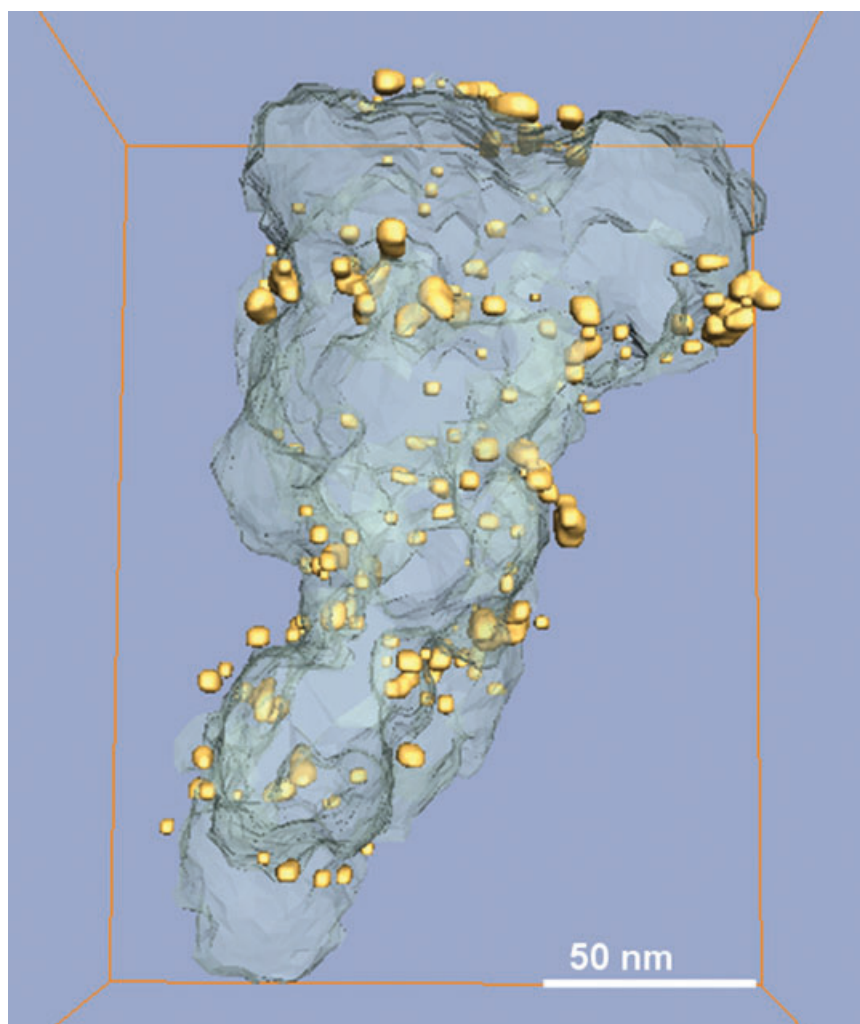


Fig. 7. Tomographic reconstruction of PtCr nanoparticles on carbon black. Most of the particles are on the surface of the carbon matrix. Acquisition parameters: Start tilt: -74.00° ; Stop tilt: $+75.00^\circ$; Tilt step: 2.00° ; Exposure time: 15 s; Magnification = 450 kx; Camera length/semi-angle: 200/40 mm/mrad; Reconstruction: SIRT (15 iter.); Visualization: Isosurface + segmentation.

Different treatments of the Pt/C or PtCr/C system affect its reactivity. For instance, the effect of temperature can lead to a phase transition of the carbon matrix from amorphous to graphitic. It is of interest to study the local structure of the carbon matrix and to correlate its degree of graphitization with parameters such as the dispersion, size or encapsulation of the supported metallic particles. Energy-filtered TEM (EFTEM) electron tomography may be used to provide such information. Gass *et al.* (2006) acquired a series of plasmon-loss images at successive tilt angles and obtained high-contrast tomographic reconstructions of composites of carbon nanotubes in a polymer matrix, allowing two carbonaceous components to be differentiated from each other. This work relied on the fact that the volume plasmon energy is known to vary between different forms of carbon: amorphous carbon has a plasmon energy of 24 eV, whereas graphitic carbon has

a plasmon energy of 27 eV (Daniels *et al.*, 2003). The ratio of two images acquired at these energies is then very sensitive to changes in carbon bonding, and can be used readily to differentiate between graphitic and amorphous carbon. Moreover, the ratio method successfully removes unwanted diffraction contrast, and for thicknesses below the mean free path, the signal increases monotonically with specimen thickness (satisfying the 'projection requirement' required for tomographic reconstruction) (Gass *et al.*, 2006). The low-loss region provides also a scattering signal that is many orders of magnitude larger than for core-loss EFTEM, and acquisition times and beam damage are therefore lower. All of these characteristics make plasmon ratio imaging suitable for tomographic reconstruction of different phases of carbon supports in future studies of supported catalysts.

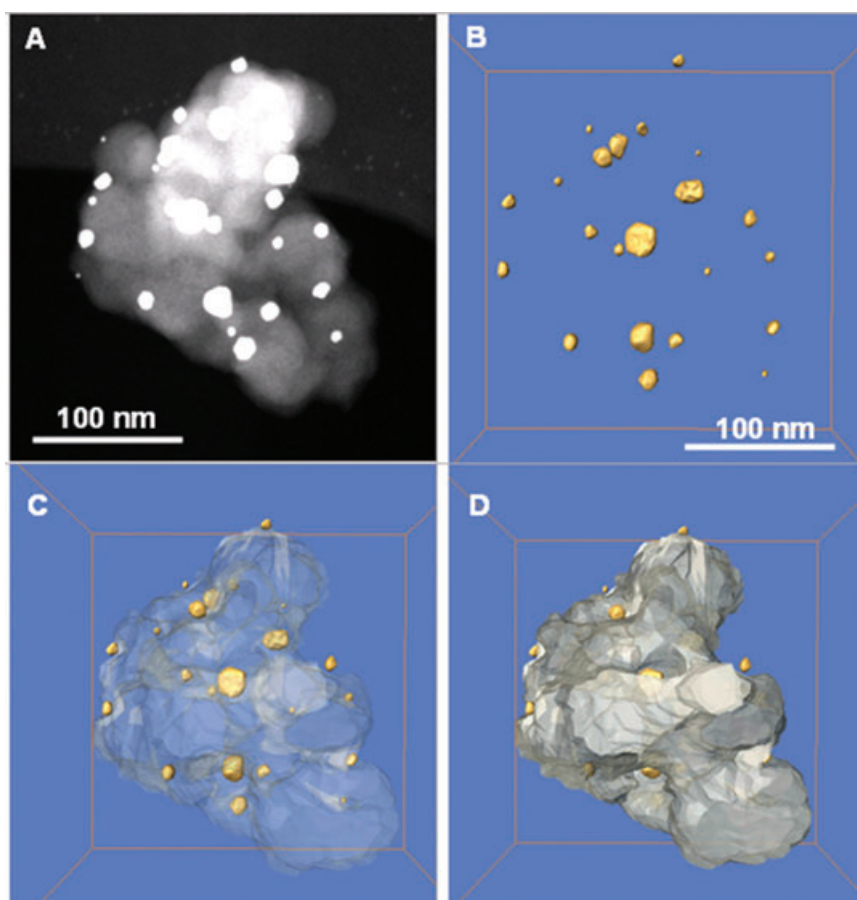


Fig. 8. Tomographic reconstruction of PtCr nanoparticles on carbon black. (A) HAADF image from the original tomographic tilt series. (B) Isosurface visualization of the PtCr particles after reconstruction. (C) Surface segmentation of the carbon support and particles. (D) As for (C) but after increasing the opacity of the matrix. Acquisition parameters: Start tilt: -65.00° ; Stop tilt: $+75.00^\circ$; Tilt step: 2.00° ; Exposure Time: 15 s; Magnification = 320 kx; Camera length/semi-angle: 490/10 mm/mrad; Reconstruction: SIRT (15 iter.); Visualization: Isosurface + segmentation.

Conclusions

Our results show that electron tomography provides important information that is complementary to high-resolution lattice imaging. Both techniques are required to understand fully the nature and role of the surfaces of faceted catalyst particles. It has been shown that HAADF STEM tomography can be used to measure the shapes of metallic catalyst nanoparticles with sizes down to 5 nm. The Pt particles examined here are found to be faceted. Rounded particle edges visible in the reconstructions are thought to result in part from the presence of small low-index (e.g. 110-type) facets, steps and terraces, and in part from artefacts and limited resolution of the tomographic reconstruction. By choosing an appropriate value of the detector inner cut-off semi-angle, STEM tomography has also been used to provide the spatial distributions of PtCr particles on carbon, for which the majority of the particles are determined to be on the

surface of the support. The positions of the catalyst particles on their support can be measured most accurately and with fewer artefacts if the difference in atomic number between the particles and the support is not too high. By contrast, the morphologies of the individual particles can be measured most accurately if their atomic number is much larger than that of the support.

Acknowledgements

The authors thank the EPSRC (UK) and the ESTEEM project for funding, and Steve Spratt, Gregory Goodlet, Tim Hyde and Peter Ash from Johnson Matthey. Thanks are due to Paul A. Midgley of the Department of Materials Science and Metallurgy in Cambridge (UK), and Angus I. Kirkland and Crispin J.D. Hetherington of the Department of Materials, Oxford (UK) for discussions and for facilitating access to their microscopy facilities.

References

- Arslan, I., Yates, T.J.V., Browning, N.D. & Midgley, P.A. (2005) Embedded nanostructures revealed in three dimensions. *Science* **309**, 2195–2198.
- Ascencio, J., Gutiérrez-Wing, C., Espinosa, M., Matin, M., Tehuacanero, S., Zorrilla, C. & José-Yacamán, M. (1998) Structure determination of small particles by HREM imaging: theory & experiment'. *Surf. Sci.* **396**, 349–368.
- Barnard, J.S., Sharp, J., Tong, J.R., & Midgley, P.A. (2006) High-resolution three-dimensional imaging of dislocations. *Science* **313**, 319.
- Bell, A.T. (2003) The impact of nanoscience on heterogeneous catalysis. *Science* **299**, 1688–1691.
- Bowker, M. (1998) *The Basis and Applications of Heterogeneous Catalysis*. Oxford University Press, Oxford.
- Burden, A.P., Baigrie, S. & Hutchison, J.L. (1998) An investigation of the electron irradiation of carbon blacks in various gas atmospheres using a modified electron microscope. *J. Microsc.* **192**, 7–19.
- Buseck, P.R., Dunin-Borkowski, R.E., Devouard, B. *et al.* (2001) Magnetite morphology and life on Mars. *Proc. Natl. Acad. Sci. U S A* **98**, 13490–13495.
- Crowther, R.A., DeRosier, D.J. & Klug, A. (1970) The reconstruction of a three-dimensional structure from projections and its application to electron microscopy. *Proc. R. Soc. Lond.* **317**, 319–340.
- Daniels, H.R., Brydson, R., Brown, A. & Rand, B. (2003) Quantitative valence plasmon mapping in the TEM: viewing physical properties at the nanoscale. *Ultramicroscopy* **96**, 547–558.
- Friedrich, H., McCartney, M.R. & Buseck, P.R. (2005) Comparison of intensity distributions in tomograms from BF TEM, ADF STEM, HAADF STEM, and calculated series. *Ultramicroscopy* **106**, 18–27.
- Gass, M.H., Koziol, K.K.K., Windle, A.H. & Midgley, P.A. (2006) Four-dimensional spectral tomography of carbonaceous nanocomposites. *Nano Lett.* **6**, 376–379.
- Gontard, L.C., Dunin-Borkowski, R.E., Chong, R.K.K., Ozkaya, D. & Midgley, P.A. (2005) Electron tomography of Pt catalyst particles and their carbon support. *J. Phys. Conf. Ser.* **26**, 203–206.
- Gontard, L.C., Chang, L.-Y., Hetherington, C.J.D., Kirkland, A.I., Ozkaya, D. & Dunin-Borkowski, R.E. (2007) Aberration-corrected imaging of active sites on industrial catalyst nanoparticles. *Angew. Chem. Int. Ed.* **47**, 3683–3685.
- Graoui, H., Giorgio, S. & Henry, C.R. (1998) Shape variations of Pd particles under oxygen adsorption. *Surf. Sci.* **417**, 350–360.
- Heidenreich, R.D., Hess, W.M. & Ban, L.L. (1968) A test object and criteria for high resolution electron microscopy. *J. App. Crystallogr.* **1**, 1–19.
- Howie, A. & Marks, L.D. (1984) Elastic strains and the energy balance for multiply twinned particles. *Philos. Mag. A* **49**, 95–109.
- Jinnai, H., Hasegawa, H., Nishikawa, Y., Sevink G.J.A., Braunfeld, M.B., Agard, D.A. & Spontak, R.J. (2006) 3D nanometer-scale study of coexisting bicontinuous morphologies in a block copolymer/homopolymer blend. *Macromol. Rapid Commun.* **27**, 1424–1429.
- Kolasinski, K.W. (2004) *Surface Science. Foundations of Catalysis and Nanoscience*, John Wiley & Sons, New York, NY.
- Marks, L.D. (1983) Modified Wulff construction for twinned particles. *J. Cryst. Growth* **61**, 556–566.
- Marks, L.D. (1984) Direct atomic imaging of solid surfaces. *Surf. Sci.* **139**, 281–298.
- Marks, L.D. (1985) Particle size effects on Wulff constructions. *Surf. Sci.* **150**, 358–366.
- Marks, L.D. (1994) Experimental studies of small particle structures. *Rep. Prog. Phys.* **57**, 603–649.
- Marks L.D. & Smith D.J. (1983) Direct surface imaging in small metal particles. *Nature* **303**, 316–317.
- Midgley, P.A., Weyland, M., Yates, T.J.V., Arslan, I., Dunin-Borkowski, R.E. & Thomas J.M. (2006) Nanoscale scanning transmission electron tomography. *J. Microsc.* **223**, 185–190.
- Midgley, P.A., Ward, E.P.W., Hungria, A.B. & Thomas, J.M. (2007) Nanotomography in the chemical, biological and materials sciences. *Chem. Soc. Rev.* **36**, 1477–1494.
- Möbus, G. & Inkson, B.J. (2001) Three-dimensional reconstruction of buried nanoparticles by element-sensitive tomography based on inelastically scattered electrons. *App. Phys. Lett.* **79**, 1369–1371.
- Ozkaya, D., Thompsett, D., Goodlet, G., Spratt, S., Ash, P. & Boyd, D. (2003) Characterisation of C supported Pt nano-particles using HREM. *Inst. Phys. Conf. Ser.* **179**, 127–130.
- Ralph, B.T.R. & Hogarth, M.P. (2002) Catalysis for low-temperature fuel cells. Part II: the anode challenges. *Platinum Met. Rev.* **46**, 146–164.
- Sattler, M.L. & Ross, P.N. (1986) The surface structure of Pt crystallites supported on carbon black. *Ultramicroscopy* **20**, 21–28.
- Topsoe, H. (2003) Developments in operando studies and in situ characterization of heterogeneous catalysts. *J. Catal.* **216**, 155–164.
- Uchida, H., Song, J.M., Suzuki, S., Nakazawa, E., Baba, N. & Watanabe, M. (2006) Electron tomography of nafion ionomer coated on Pt/carbon black in high utilization electrode for PEMFCs. *J. Phys. Chem. B* **110**, 13319–13321.
- Van de Waal, B.W. (1996) Cross-twinning model of fcc crystal growth. *J. Cryst. Growth* **158**, 153–165.
- Wang, T., Lee, C. & Schmidt, L.D. (1985) Shape and orientation of supported Pt particles. *Surf. Sci.* **163**, 181–197.
- Wang, Y., Teitel, S. & Dellago, C. (2004) Melting and equilibrium shape of icosahedral gold nanoparticles. *Chem. Phys. Lett.* **394**, 257–261.
- Weyland, M. (2002) Electron tomography of catalysts. *Top. Catal.* **21**, 175–183.
- Weyland, M., Midgley, P.A. & Thomas, J.M. (2001) Electron tomography of nanoparticle catalysts on porous supports: a new technique based on Rutherford scattering. *J. Phys. Chem. B* **105**, 7882–7886.
- Weyland, M., Yates, T.J.V., Dunin-Borkowski, R.E., Laffont, L. & Midgley, P.A. (2006) Nanoscale analysis of three-dimensional structures by electron tomography. *Scripta Mater.* **55**, 29–33.
- Wikander K., Hungria, A.B., Midgley P.A., Palmqvist E.C., Holmberg K. & Thomas J.M. (2007) Incorporation of platinum nanoparticles in ordered mesoporous carbon. *J. Colloid Interface Sci.* **305**, 204–208.
- Xu, X., Peng, Y., Saghi, Z., Gay, R., Inkson, B.J. & Möbus, G. (2007a) 3D reconstruction of SPM probes by electron tomography. *J. Phys. Conf. Ser.* **61**, 810–814.
- Xu, X., Saghi, Z., Gay, R. & Möbus, G. (2007b) Reconstruction of 3D morphology of polyhedral nanoparticles. *Nanotechnology* **18**, 1–8.
- Yacamán, M.J. & Domínguez, J.M. (1980) Characterization of small platinum particles supported on graphite by electron microscopy. *J. Catal.* **64**, 213–222.
- Yang, C., Zhang, H.-B., Li, J.-J. & Takaoka, A. (2005) The top-bottom effect of a tilted thick specimen and its influence on electron tomography. *J. Elec. Microsc.* **54**, 367–371.
- Yurtsever, A., Weyland, M. & Muller, D.A. (2006) Three-dimensional imaging of nonspherical silicon nanoparticles embedded in silicon oxide by Plasmon tomography. *App. Phys. Lett.* **89**, 151920.